






Article

Magnetic and Luminescent Properties of Isostructural 2D Coordination Polymers Based on 2-Pyrimidinecarboxylate and Lanthanide Ions

Amalia García-García ¹, Andoni Zabala-Lekuona ² , Ainhoa Goñi-Cárdenas ¹, Javier Cepeda ² , José M. Seco ², Alfonso Salinas-Castillo ³ , Duane Choquesillo-Lazarte ^{4,*}  and Antonio Rodríguez-Diéguez ^{1,*} 

¹ Department of Inorganic Chemistry, Faculty of Science, University of Granada, 18071 Granada, Spain; amaliagarcia@correo.ugr.es (A.G.-G.); 7991ainhoa@gmail.com (A.G.-C.)

² Department of Applied Chemistry, Chemistry Faculty, University of the Basque Country (UPV/EHU), 20018 Donostia-San Sebastián, Spain; andoni.zabala@ehu.es (A.Z.-L.); javier.cepeda@ehu.es (J.C.); josemanuel.seco@ehu.es (J.M.S.)

³ Department of Analytical Chemistry, Faculty of Science, University of Granada, 18071 Granada, Spain; alfonso@ugr.es

⁴ Laboratorio de Estudios Cristalográficos, IACT, CSIC-Universidad de Granada, Avda. de las Palmeras 4, 18100 Armilla, Spain

* Correspondence: duane.choquesillo@csic.es (D.C.-L.); antonio5@ugr.es (A.R.-D.)

Received: 29 May 2020; Accepted: 30 June 2020; Published: 2 July 2020



Abstract: A couple of isostructural coordination polymers with the general formula $[Ln_4(pymca)_4(AcO)_8]_n$ have been obtained from reactions between pyrimidine-2-carboxylate (pymca) ligand and rare-earth ions ($Ln = Dy$ (**1**), Nd (**2**)). These two-dimensional compounds have been characterized and the crystal structures have been solved by single-crystal X-ray diffraction technique, resulting in layers along the bc plane based on pymca and acetate anions that act as bridging ligands between metal atoms. Given that pymca and acetate anions possess carboxylate and hetero-nitrogen groups, it is possible to build a coordination polymer whose metal centers have a nine coordination. Furthermore, static and dynamic magnetic measurements of compound **1** reveal the lack of single molecule-magnet (SMM) behavior in this system due to the following two effects: (i) the ligand field does not stabilize magnetic ground states well separated from excited states, and (ii) anisotropy axes are not collinear, according to results with Magellan software. On another level, luminescent properties of compounds **1** and **2** are attributed to singlet $\pi-\pi^*$ transitions centered on pymca ligand as corroborated by time-dependent density functional theory (TD-DFT) calculations.

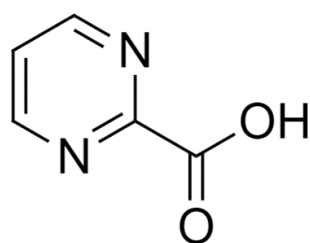
Keywords: coordination polymer; pyrimidine-2-carboxylate; lanthanide; luminescence; magnetism

1. Introduction

Coordination polymers (CPs) are defined as infinite systems built up from metal ions and organic ligands linked via coordination bonds and other weak chemical bonds such as hydrogen bonds, $\pi-\pi$ stacking, or van der Waals interactions [1]. These materials have gained considerable attention in recent decades, in particular, lanthanide-based coordination polymers, due to their varied structures [2,3], high coordination numbers, gas storage properties [4], biochemical and medical applications [5], as well as interesting luminescent [6] and magnetic properties [7–9]. The key factor for the synthesis of CPs is to choose appropriate metal centers and bridging ligands to obtain the desired topologies and properties, although other factors can also have an influence such as metal-to-ligand ratio, temperature, pH value, and solvents [10,11]. Among ligands, with the goal to achieve coordination

frameworks based on *f*-block metal centers with local connectivity numbers larger than six, ligands containing both carboxylate groups and hetero-nitrogen chemical functions have been extensively used in the construction of these novel systems because both groups can coordinate to metal centers in different ways [12–14].

Ligands such as pyridylcarboxylate, imidazolylcarboxylate, pyrimidylcarboxylate, or indolylcarboxylate derivatives are used extensively in coordination chemistry based on lanthanide ions [15–17]. Specifically, we chose the ligand pyrimidine-2-carboxylate (pymca), which contains both oxygen and nitrogen coordination atoms (Scheme 1), because, to date, only a few structures based on rare-earth ions and this ligand have been reported, all of them by Wang et al. [8]. Inspired by all the above-mentioned ideas, we decided to react pymca and lanthanide ions with the objective of building coordination polymers with interesting luminescent and magnetic properties, due to the fact that, fifteen years ago, we were the pioneers to design and work with this novel ligand, which shows great ability to form two-dimensional and three-dimensional coordination polymer compounds. In this way, we were able to obtain a great variety of multidimensional coordination polymers with interesting magnetic and luminescent properties effectively explained by density functional theory (DFT)-type calculations [18–21].



Scheme 1. Pyrimidine-2-carboxylic acid (pymca) ligand.

In this paper, we reported the synthesis and characterization of two isostructural two-dimensional coordination polymers based on lanthanide ions, mixed pyrimidine-2-carboxylate, and acetate anions as ligands with the general formula $[\text{Ln}_4(\text{pymca})_4(\text{AcO})_8]_n$ ($\text{Ln} = \text{Dy}$ (**1**), Nd (**2**)). Their magnetic and luminescent properties were also investigated and corroborated by theoretical calculations.

2. Materials and Methods

2.1. Synthesis

All starting reagents were purchased from commercial sources (Sigma-Aldrich) and were used as received and without additional purification.

2.1.1. Synthesis of $[\text{Dy}_4(\text{pymca})_4(\text{AcO})_8]_n$ (**1**)

Compound **1** was obtained following a solvothermal route through the following procedure: First, 0.020 g (0.19 mmol) of 2-pyrimidinecarbonitrile, in situ precursor of pymca ligand, was dissolved in 1 mL of *N,N*-dimethylformamide (DMF). In a separate vial, 0.0215 g (0.063 mmol) of $\text{Dy}(\text{AcO})_3$ was dissolved in 0.5 mL of distilled water. Metal solution was added dropwise to the ligand solution. The resulting mixture was stirred and heated at 100 °C for 24 h. After this time, white crystals of **1** for single crystal X-ray diffraction were obtained during the heating process under autogenous pressure. Anal. Calcd. for $\text{C}_{18}\text{H}_{18}\text{Dy}_2\text{N}_4\text{O}_{12}$: C, 26.76; H, 2.25; N, 6.94%. Found: C, 26.54; H, 2.13; N, 7.02%. FT-IR: 1620 cm^{-1} (m), 1568 cm^{-1} (s), 1413 cm^{-1} (s), 1373 cm^{-1} (s).

2.1.2. Synthesis of $[\text{Nd}_4(\text{pymca})_4(\text{AcO})_8]_n$ (**2**)

Compound **2** was synthesized following a similar procedure as follows: First, 0.015 g (0.142 mmol) of 2-pyrimidinecarbonitrile ligand was dissolved in 0.5 mL of DMF. In a separate vial, 0.0155 g (0.047 mmol) of $\text{Nd}(\text{AcO})_3 \cdot \text{H}_2\text{O}$ was also dissolved in 0.5 mL DMF. Metal solution was added to the

ligand solution. The reaction solution was stirred and heated at 100 °C for 24 h. X-ray quality white crystals of **2** were obtained. Anal. Calcd. for $C_{18}H_{18}Nd_2N_4O_{12}$: C, 28.03; H, 2.35; N, 7.27%. Found: C, 27.96; H, 2.28; N, 7.33%. FT-IR: 1622 cm^{-1} (m), 1560 cm^{-1} (s), 1419 cm^{-1} (s), 1373 cm^{-1} (s).

2.2. Characterization Methods

2.2.1. Physico-Chemical Characterization

Elemental analyses (C, H, and N) were carried out at the “Centro de Instrumentación Científica” (University of Granada) on a THERMO SCIENTIFIC analyzer model Flash 2000. The FTIR spectra were recorded with a BRUKER TENSOR 27 FT-IR and OPUS data collection program.

2.2.2. Single-Crystal X-Ray Diffraction

Measured crystals were prepared under inert conditions immersed in perfluoropolyether as protecting oil for manipulation. Suitable crystals were mounted on MiTeGen Micromounts™, and these samples were used for data collection. Data for **1** and **2** were collected with a Bruker D8 Venture diffractometer with a Photon detector equipped with graphite monochromated $MoK\alpha$ radiation ($\lambda = 0.71073 \text{ \AA}$). The data were processed with APEX3 suite [22]. The data contain monoclinic pseudo-translational symmetry. This results in a pseudo C-centered cell (Bravais centering), but the data clearly show that the reflections with $h + k = \text{odd}$ are weak but definitely not extinct, therefore, P-centered cell was chosen. Looking at the systematic absences, there is clearly a 2_1 screw axis along the crystallographic b-axis. Additionally, there are indications for the presence of a-, n-, and c-glide planes. There are some violations of reflection conditions for the glide planes. The structures were solved in space group $P2_1$ and refined as inversion twins. The packing consisted of two symmetry-independent coordination planes parallel to the bc plane. The structures were solved by Intrinsic Phasing using the ShelXT program [23], which revealed the position of all non-hydrogen atoms. These atoms were refined on F^2 by a full-matrix least-squares procedure using anisotropic displacement parameters [24]. All hydrogen atoms were located in difference Fourier maps and included as fixed contributions riding on attached atoms with isotropic thermal displacement parameters 1.2 or 1.5 times those of the respective atom. The OLEX2 software was used as a graphical interface [25]. As a consequence of the pseudo-symmetries, the least-squares refinements of the structures were not stable, and the use of restraints was required. Some ISOR and RIGU commands had to be used to obtain reasonable displacement parameters for selected non-hydrogen atoms. The Addsym routine implemented in the program PLATON [26] found a $P2_1/c$ symmetry. The two symmetry-independent coordination planes were maintained in the higher symmetry, but refinement in $P2_1/c$ was not successful. Clearly, the $P2_1$ solution describes the structure better than in the $P2_1/c$ space group, being the inversion center a pseudo-symmetry operator. The crystallographic data for the reported structures were deposited with the Cambridge Crystallographic Data Center as supplementary publication no. CCDC 2006485 and 2006486. Additional crystal data are shown in Table 1. Copies of the data can be obtained free of charge at <http://www.ccdc.cam.ac.uk/products/csd/request>.

2.2.3. Magnetic Measurements

Magnetic susceptibility measurements were performed on polycrystalline samples of the complexes with a Quantum Design SQUID MPMS-7T susceptometer at an applied magnetic field of 1000 Oe. The susceptibility data were corrected for the diamagnetism, the temperature-independent paramagnetism, and the magnetization of the sample holder. Ac measurements were performed on a Quantum Design Physical Property Measurement System Model 6000 magnetometer under a 3.5 G ac field and frequencies ranging from 60 to 10,000 Hz.

Table 1. Crystallographic data and structure refinement details of compounds **1** and **2**.

Compound	1	2
Formula	C ₁₈ H ₁₈ N ₄ O ₁₂ Dy ₂	C ₁₈ H ₁₈ N ₄ O ₁₂ Nd ₂
M _r (g mol ⁻¹)	807.36	770.84
Crystal system	Monoclinic	Monoclinic
Space group	P2 ₁	P2 ₁
Temperature (K)	298(2)	100
a (Å)	15.0967(7)	15.1628(7)
b (Å)	9.3786(4)	9.5069(4)
c (Å)	16.4416(8)	16.6857(8)
α (°)	90	90
β (°)	103.8920(10)	104.791(2)
λ (°)	90	90
V (Å ³)	2259.81(18)	2325.56(18)
Z	4	4
ρ (g cm ⁻³)	2.373	2.202
μ (mm ⁻¹)	6.635	4.487
Unique reflections	10,291	7722
R _{int}	0.057	0.088
GoF ^a	1.119	1.023
R1 ^b /wR2 ^c [I > 2σ(I)]	0.0590/0.1481	0.0750/0.1740
R1 ^b /wR2 ^c [all data]	0.0823/0.1624	0.1279/0.2049

^a R₁ = Σ|F_o - |F_c||/Σ|F_o|; ^b values in parentheses for reflections with I > 2σ(I); ^c wR₂ = {Σ[w(F_o² - F_c²)²]/Σ[w(F_o²)²]}^{1/2}.

2.2.4. Luminescent Measurements

Fluorescence emission spectra were recorded at room temperature using polycrystalline samples in a Varian Cary Eclipse fluorescence spectrofluorimeter equipped with a xenon discharge lamp (peak power equivalent to 75 kW), Czerny–Turner monochromators, and an R-928 photomultiplier tube. The emission spectra were recorded in the visible region (300–700 nm), the photomultiplier detector voltage was fixed at 550 V, and the excitation and emission slits were set both at 5 nm.

2.2.5. Computational Details

The computational strategy adopted to calculate the magnetic coupling constant (J_{calc}) values corresponds to the broken symmetry strategy and has been described and validated elsewhere [27]. One calculation was performed to determine the high-spin state and another to determine the low-spin broken symmetry state, using Gaussian 16 package [28]. The correctness of the latter state was ensured by means of its spin density distribution. These calculations were performed using density functional theory (DFT) with hybrid B3LYP functional and Gaussian-implemented 6-311G(d) basis set for all non-metallic atoms, whereas the corresponding LANL2DZ pseudopotentials were used for the metal atoms. Spin-density surfaces were plotted using GaussView 5 [29]. The anisotropy axis of the Dy³⁺ ions was calculated with Magellan software [30]. Regarding the calculations of the PL spectrum of pymca ligand, it was carried out by time-dependent density functional theory (TD-DFT) methodology with Gaussian 16 package, using equivalent model chemistries detailed for broken symmetry calculations. The 40 lowest excitation states were calculated by the TD-DFT method. Results were analyzed with GaussSum program package [31] and molecular orbitals (MOs) plotted using GaussView 5.

3. Results and Discussion

Pyrimidine-2-carboxylic acid ligand allowed the formation of two isostructural coordination polymers by varying the metal center. Thus, the solvothermal reaction of the pymca with dysprosium(III) and neodymium(III) acetate hydrate in DMF/H₂O mixture with a 3:1 molar ratio afforded two-dimensional metal-organic frameworks.

3.1. Crystal Structure of $[Ln_4(pymca)_4(AcO)_8]_n$ ($Ln = Dy$ (1), Nd (2))

Compounds **1** and **2** are isostructural with the monoclinic space group $P2_1$, therefore, just compound $[Dy_4(pymca)_4(AcO)_8]_n$ (**1**) is described in detail.

The crystal structure of complex **1** consists of a two-dimensional coordination polymer with mixed acetate and pymca bridging ligands. The asymmetric unit is based on two units with two Dy^{3+} cations, two pymca ligands, and four acetate anions each one (Figure 1). Dy1, Dy3, and Dy4 atoms are coordinated with five oxygen atoms from four acetate anions and two nitrogen and two oxygen atoms belonging to two pymca ligands to complete a nine-coordination environment DyN_2O_7 that resembles a muffin polyhedron (see Figure S1 in Supplementary Materials). Instead, the coordination number drops to eight for the Dy2 atom despite its equivalent environment, hence showing a less distorted square antiprism, owing to the fact that one of the $Dy-O_{acetate}$ bond distance is too large (ca. 2.98 Å) as to be considered a coordination bond (see Section S3 in Supplementary Materials).

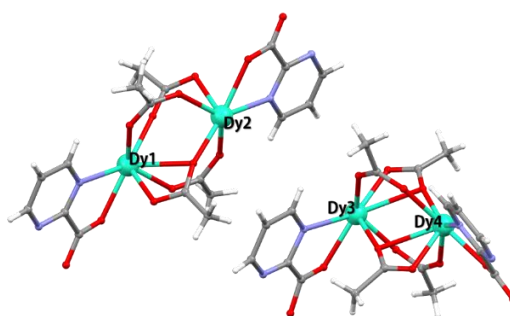


Figure 1. View of the asymmetric unit of compound **1**.

The structure consists of two similar layers parallel to the bc plane. They are not equal, since each one contains two chemically equivalent but crystallographically different Dy atoms (one layer is composed of Dy1 and Dy2 atoms, meanwhile the other one is made up of Dy3 and Dy4 atoms) (Figure 2). Selected bond lengths and angles of coordination spheres are not the same in the two layers, so they are all included in Tables S1–S4 for compounds **1** and **2**.

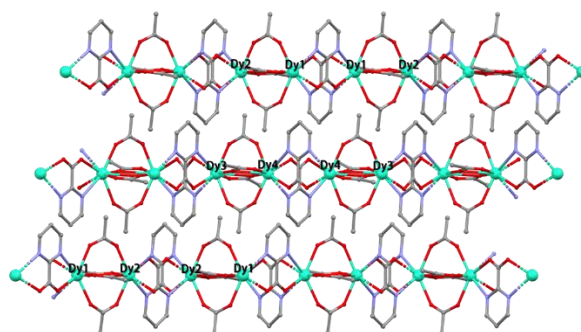


Figure 2. Perspective view along the b -axis of the two independent two-dimensional layers present in compound **1**.

Within the structure, both pymca and acetate anions act as bridging ligands by joining metal atoms, resulting in two different distance ranges of 6.472(2)–6.480(2) and 3.952(2)–4.087(2) Å, respectively. The shorter range of distances corresponds to inequivalent metal bonds, e.g., Dy3–Dy4 bond, and the largest one belongs to bonds between equal metal atoms, e.g., Dy3–Dy3 bond. The anionic pymca ligands coordinate in a bisbidentate form to metal atoms. In contrast, the acetate anions show two different coordination modes. Those two anions that lie out perpendicular to the bc plane show a $\mu-\kappa O:\kappa O'$, while the other two acetate anions arrange parallel to the bc plane and create a $\mu-\kappa^2 O, O':\kappa O$ coordination between two Dy^{3+} atoms [32].

This arrangement of the ligands produces mesh shaped two-dimensional layers in the bc plane whose holes are occupied by acetate ligands (Figure 3a). A summary of the structure refinements of compounds 1 and 2 is given in Table 1.

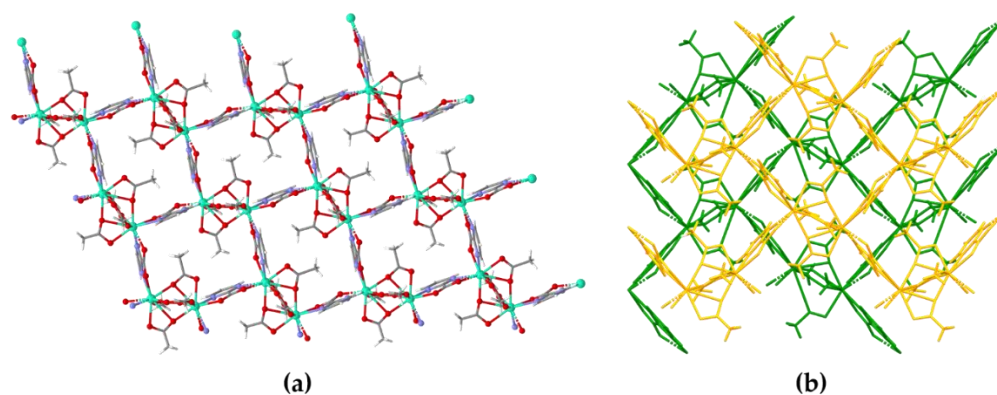


Figure 3. View of layers along the a-axis extended in the bc plane of compound 1. (a) One layer in which it is possible to see the voids occupied by two acetate ligands; (b) Layers superimpose in a zig-zag arrangement, so there are no pores in the three-dimensional structure.

3.2. Magnetic Properties of Compound 1

3.2.1. Static Magnetic Measurements

The static magnetic properties of compound 1 were investigated by direct current (dc) magnetic susceptibility measurements in the 2–300 K temperature range under an applied field of 1000 Oe (Figure 4).

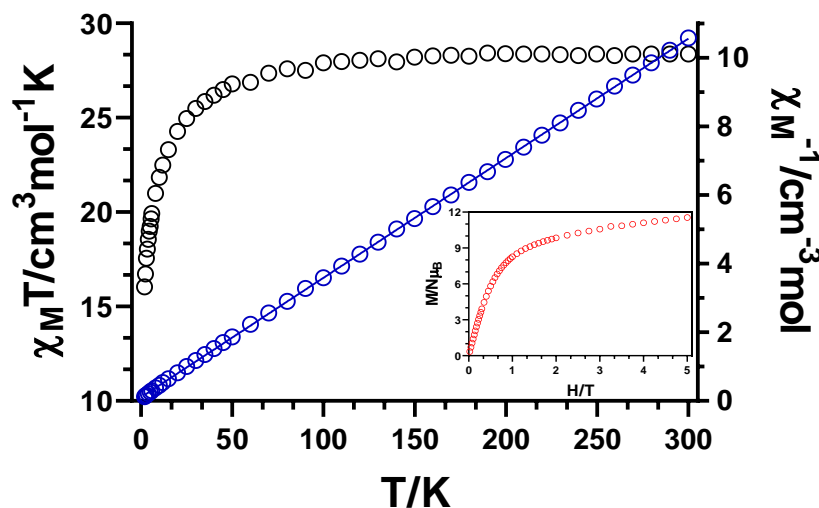


Figure 4. Temperature dependence of the $\chi_M T$ product (colour black) and $1/\chi_M$ (colour blue) versus T for 1 in the 2–300 K range. The solid line represents the best fitting with the Curie–Weiss law. Inset: Magnetization vs. H plot recorded at 2.0 K.

The $\chi_M T$ vs. T plot (Figure 4, black dots) reveals a value of $28.37 \text{ cm}^3 \text{ K mol}^{-1}$ at room temperature, which is in good agreement with the expected value of $28.34 \text{ cm}^3 \text{ K mol}^{-1}$ for two non-interacting Dy^{3+} ions in the free-ion approximation ($4f^9$, $J = 15/2$, $S = 5/2$, $L = 5$, $g = 4/3$ $^6\text{H}_{15/2}$). Upon cooling down from room temperature, the $\chi_M T$ value remains almost unchanged until nearly 50 K, where it starts to fall abruptly reaching a minimum value of $16.04 \text{ cm}^3 \text{ K mol}^{-1}$ at 2.0 K. This drop could be associated with diverse effects. On the one hand, the thermal depopulation of the Stark sublevels resulting from crystal-field effects provoke this decrease in $\chi_M T$ but, on the other hand, there could also be weak

antiferromagnetic interactions between the two Dy^{3+} ions provided by carboxylate bridges of the pymca ligands. The strong spin-orbit coupling present in the Dy^{3+} ions complicates the treatment of the data in order to obtain the coupling exchange constant J . However, with the aim of shedding some light regarding the nature of the metal–metal interactions, we opted to follow the next approach. First, we studied the magnetic data in the same temperature range by using the Curie–Weiss law, namely $1/\chi = (T - \theta)/C$ (Figure 4, blue dots and line). The fitting afforded C and θ values of $28.69 \text{ cm}^3 \text{ K mol}^{-1}$ and -2.9 K , respectively. The low negative value of θ indicates the presence of weak intramolecular antiferromagnetic interactions suggesting that the lowering of the χ_{MT} value is not solely influenced by the depopulation of the Stark sublevels. In addition, with the purpose of supporting these results and better estimating the nature of the magnetic exchange interactions, we conducted DFT calculations with the broken symmetry methodology [33]. In order to do that, two different dimeric fragments were considered separately with the aim of evaluating the two possible superexchange pathways found in the compound. The first selected dinuclear entity evaluates the interactions within the paddle-wheel shaped fragment involving four bridging acetate groups (inside it a short $\text{Ln}\cdots\text{Ln}$ distance of ca. 4.0 \AA is established), whereas the second entity involves the bidentate pymca bridging ligand (this establishes a longer $\text{Ln}\cdots\text{Ln}$ distance about 6.5 \AA). As mentioned, the strong spin-orbit coupling of the Dy^{3+} ions complicated the calculation, thus, the anisotropic ions were replaced by isotropic Gd^{3+} ones in order to have a good estimation of the J parameter. In both superexchange pathways, a negligible coupling constant was calculated (Figure 5). Therefore, we conclude that the decay in the χ_{MT} value arises mainly from the depopulation of the Stark sublevels and besides intramolecular interactions insignificantly contribute to it.

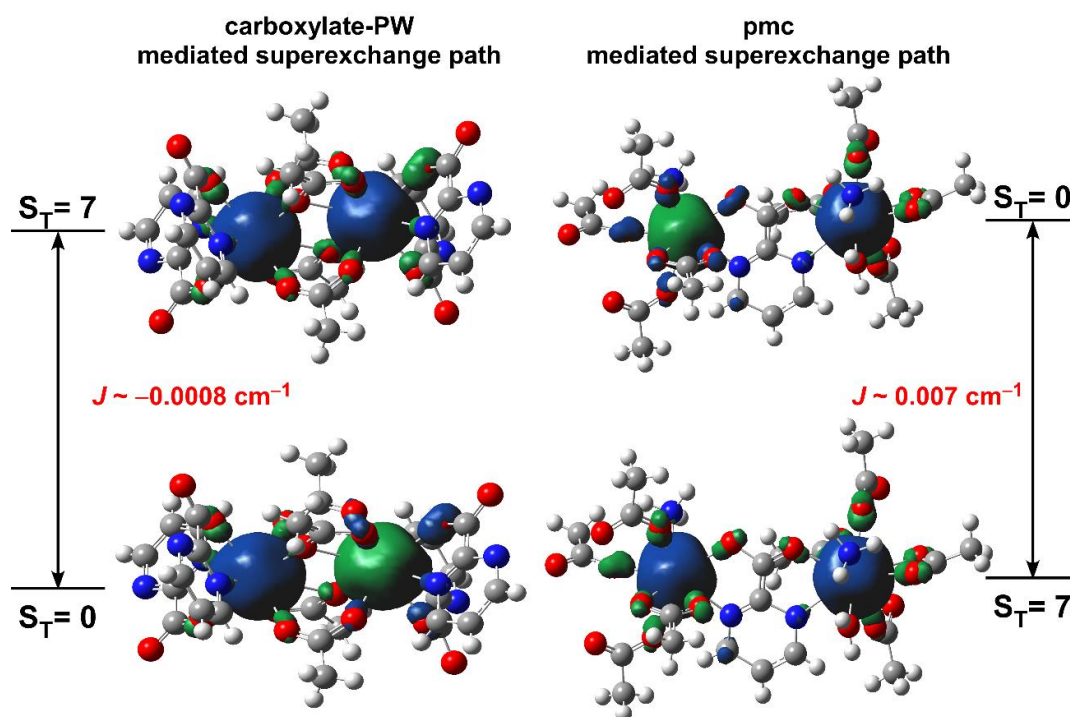


Figure 5. Broken symmetry DFT based calculation on an isostructural model grown with Dy^{3+} centers to account for the value of the exchange parameter. Spin densities are shown for ground and excited states involving the two superexchange pathways.

The $M(H)$ plot was also recorded at 2 K , which is shown in the inset of Figure 4. The magnetization value rapidly increases with field strength up to 1 T , above it a gradual increase is observed reaching a maximum value of $11.54 N_{\mu_B}$, at 5 T . This gradual increase and the low “saturation” value, which is far lower than the expected value of $19.9 N_{\mu_B}$ expected for two Dy^{3+} ions suggests significant magnetic anisotropy.

3.2.2. Dynamic Magnetic Properties

In view of the fact that highly anisotropic lanthanides such as Dy^{3+} are potential candidates to present slow relaxation of the magnetization [34], dynamic magnetic properties of **1** were studied by alternating current (ac) magnetic measurements. Firstly, measurements were carried out applying an oscillatory field of 3.5 Oe and under zero dc field. However, the out-of-phase component of the susceptibility (χ_M'') did not show any signal (Figure S1). The lack of single molecule-magnet (SMM) behavior in this case could be attributed to the fast quantum tunneling of the magnetization (QTM). It is well known [35] that the use of an external magnetic field could be a good technique in order to overcome this undesired phenomenon. Nonetheless, in this case the Dy^{3+} based compound did not show any χ_M'' signal even when applying an external magnetic field of 1 kOe. This fact indicates that either there is still a strong QTM process that the field is not able to quench, or that the system is actually a common paramagnet.

The dynamic magnetic properties of SMMs are very sensitive to the crystal field. In general, Ln^{3+} ions are divided into the following two main groups: ions with an oblate (Dy^{3+} and Tb^{3+} , for example) or prolate (Er^{3+} and Yb^{3+} , for example) electron density. The qualitative design principles proposed by Rinehart and Long [36] indicate that in order to enhance the single ion anisotropy of Dy^{3+} , and thus the SMM behavior, the negatively charged ligands are preferred to be axially coordinated. This has been proved for a wide number of Dy^{3+} systems, such as for dysprosium metallocenes or systems with pentagonal-bipyramid geometry [34,37], where the strong electron donating groups are axially coordinated to the metal ions. We believe that the lack of SMM behavior in this compound arises from the inappropriate ligand field established around the metal ions, as well as the weak exchange coupling between them. On the one hand, as mentioned in the crystal structure description, the coordination environments around the four Dy^{3+} centers are quite distorted. Noteworthy, Dy2 displays the lowest SHAPE value (see SI, Tables S5 and S6) for a square antiprism polyhedron, which has been proved to be a suitable geometry in order to stabilize the highly magnetic $m_J = \pm 15/2$ states as ground state [21]. However, in this compound, Dy2 displays nearly nine coordination and, moreover, there are not remarkably short and negatively charged Dy–O bonds that provide axially to the system. On the other hand, in a previously Dy^{3+} based MOF reported by us [38], it was shown that even in weakly exchange coupled systems, when anisotropy axes are parallel, a slower relaxation of the magnetization is enhanced. In our case, considering the dinuclear entity where both of the lanthanide ions possess the same coordination environment, the lack of an inversion center between both ions provokes a lack of parallelism between the axes (calculated by Magellan software, Figure 6). Hence, both of the mentioned effects probably account for the lack of SMM behavior in this system.

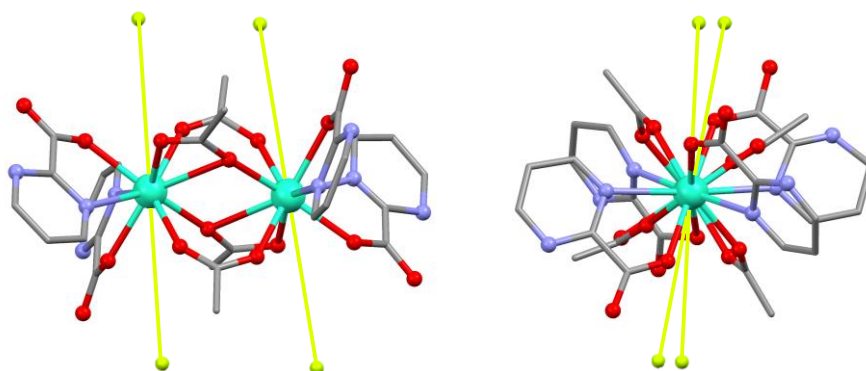


Figure 6. Two perspective views of the magnetic axes of Dy^{3+} ions calculated with the Magellan software. A reduced dinuclear fragment of the structure was considered in order to perform the calculation. Hydrogen atoms are omitted for the sake of clarity.

3.3. Luminescence Properties

As it is well-known, lanthanide-based emissions are characterized by very narrow and pure emission bands derived from the shielding of valence f shell, although, at the same time, their emission brightness tends to be low because of the low coefficients of their absorption bands [39]. Therefore, in order to obtain a luminescent compound, a ligand-to-metal charge transfer process (between ligands triplet state and excited inner states of the lanthanide(III)) must take place, which is denoted as antennae effect [40]. In this work, the luminescence properties of compounds **1** and **2** were investigated in solid state, at room temperature. Figure 7 shows the emission spectra of both complexes at $\lambda_{\text{ex}} = 240$ nm. Compounds **1** and **2** show similar emission spectra compared to that of free pymca ligand, with only one intense peak at 400 nm, which allows one unequivocally attributing the emission as ligand-centered in both compounds. The absence of any lanthanide(III)-based characteristic emission in the visible spectra, mainly for the Dy^{3+} atom in compound **1** means that the pymca ligand is not able to transfer the energy gained during the excitation process to the lanthanide atoms (i.e., there is no efficient antennae effect happening in these compounds), pymca ligand does not sensitize the lanthanide(III) ions in these compounds in such a way that only the ligand-centered emission is observed. Time-dependent DFT (TD-DFT) calculations conducted on a suitable model of the ligand reveals that the main transition occurs from the LUMO + 1 to the HOMO - 2, which can be regarded as a $\pi \leftarrow \pi^*$ transition in view of the shape of the molecular orbitals involved.

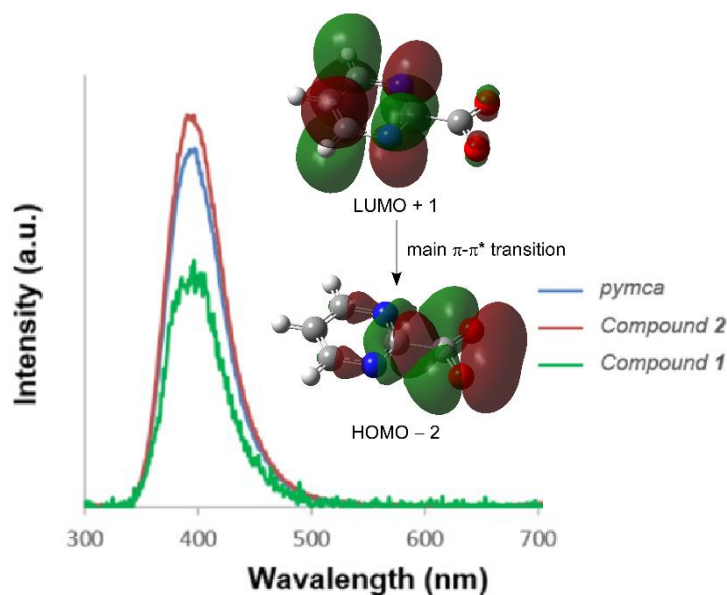


Figure 7. Emission spectra of compound **1** (green line), compound **2** (red line), and pymca ligand (blue line) at $\lambda_{\text{ex}} = 240$ nm. Inset shows the main electronic transition occurring in the ligand.

4. Conclusions

Two isostructural coordination polymers with the general formula $[\text{Ln}_4(\text{pymca})_4(\text{AcO})_8]_n$ were obtained from reactions between pyrimidine-2-carboxylate (pymca) ligand and rare-earth ions ($\text{Ln} = \text{Dy}$ (**1**), Nd (**2**)). These two-dimensional compounds were characterized resulting in layers along the bc plane based on pymca and acetate anions that act as bridging ligands between metal atoms. Regarding the magnetic properties, although highly anisotropic lanthanide ions such as Dy^{3+} were employed, we concluded that the ligand field provided by the carboxylate groups and nitrogen donor atoms was not suitable to stabilize high magnetic ground states well separated from excited states. Moreover, we find out that the anisotropy axes calculated by Magellan software are not collinear, a fact that even in weakly exchange coupled systems negatively affects the SMM behavior. Under UV excitation, both compounds exhibit a pymca ligand-centered emission based on a main

$\pi \leftarrow \pi^*$ transition, confirming the null capacity of pymca to sensitize the selected lanthanide(III) ions in the present structures. New studies in these directions are currently being carried out in our laboratory focusing, for instance, on the possible use of 3s-4f materials in electronic devices.

Supplementary Materials: The following are available online at <http://www.mdpi.com/2073-4352/10/7/571/s1>, Crystallographic Data: Table S1: Selected bond lengths (Å) for complex 1, Table S2: Selected bond lengths (Å) for complex 2, Table S3: Selected bond angles (°) for complex 1, Table S4: Selected bond angles (°) for complex 2, Figure S1. Perspective views of the Dy³⁺ ions in the crystal structure of 1. Hydrogen atoms are omitted for clarity. IR spectra: Figure S2. IR spectrum of 2-pyrimidinecarbonitrile ligand, precursor of pymca ligand, Figure S3. IR spectrum of [Dy₄(pymca)₄(AcO)₈]_n (compound 1), Figure S4. IR spectrum of [Nd₄(pymca)₄(AcO)₈]_n (compound 2). Continuous Shape Measurements for compounds: Table S5. Continuous Shape Measurements for compounds 1 and 2 considering a coordination number of 9, Table S6. Continuous Shape Measurements for Dy²⁺ in compound 1, considering its eight-coordination. Magnetic Measurements: Figure S5. Temperature dependence of in-phase (red) and out-of-phase (blue) components of the ac susceptibility in a zero (top) and under 1 kOe applied dc field (down) for 1. Photoluminescence measurements: Figure S6. Excitation spectrum for the ligand sample.

Author Contributions: Investigation, A.G.-G., A.Z.-L., A.S.-C., and A.G.-C.; data curation J.C. and J.M.S.; supervision, D.C.-L. and A.R.-D. All authors have read and agreed to the published version of the manuscript.

Funding: This research received no external funding.

Acknowledgments: Financial support was given by Junta de Andalucía (FQM-394), Red Guipuzcoana de Ciencia, Tecnología e Innovación (OF218/2018), University of the Basque Country (GIU 17/13), Gobierno Vasco/Eusko Jaurlaritza (IT1005-16), and the Spanish Ministry of Science, Innovation and Universities (MCIU/AEI/FEDER, UE) (PGC2018-102052-A-C22, PGC2018-102052-B-C21, and PGC2018-102047-B-I00). The authors thank for technical and human support provided by SGIker of UPV/EHU and European funding (ERDF and ESF). A.Z.-L. is grateful to the Government of the Basque Country for the predoctoral fellowship. The authors thank SGIker of UPV/EHU for technical and human support, and European funding (ERDF and ESF).

Conflicts of Interest: The authors declare no conflict of interest.

References

1. Robin, A.Y.; Fromm, K.M. Coordination polymer networks with O- and N-donors: What they are, why and how they are made. *Coord. Chem. Rev.* **2006**, *250*, 2127–2157. [[CrossRef](#)]
2. Sun, Y.-Q.; Zhang, J.; Chen, Y.-M.; Yang, G.-Y. Porous Lanthanide–Organic Open Frameworks with Helical Tubes Constructed from Interweaving Triple-Helical and Double-Helical Chains. *Angew. Chem. Int. Ed.* **2005**, *44*, 5814–5817. [[CrossRef](#)] [[PubMed](#)]
3. Pan, L.; Huang, X.; Li, J.; Wu, Y.; Zheng, N. Novel Single- and Double-Layer and Three-Dimensional Structures of Rare-Earth Metal Coordination Polymers: The Effect of Lanthanide Contraction and Acidity Control in Crystal Structure Formation. *Angew. Chem. Int. Ed.* **2000**, *39*, 527–530. [[CrossRef](#)]
4. Pan, L.; Adams, K.M.; Hernandez, H.E.; Wang, X.; Zheng, C.; Hattori, Y.; Kaneko, K. Porous Lanthanide–Organic Frameworks: Synthesis, Characterization, and Unprecedented Gas Adsorption Properties. *J. Am. Chem. Soc.* **2003**, *125*, 3062–3067. [[CrossRef](#)] [[PubMed](#)]
5. Tan, H.; Ma, C.; Song, Y.; Xu, F.; Chen, S.; Wang, L. Determination of tetracycline in milk by using nucleotide/lanthanide coordination polymer-based ternary complex. *J. Biosens. Bioelectron.* **2013**, *50*, 447–452. [[CrossRef](#)] [[PubMed](#)]
6. Zhao, B.; Chen, X.-Y.; Cheng, P.; Liao, D.-Z.; Yan, S.-P.; Jiang, Z.-H. Coordination Polymers Containing 1D Channels as Selective Luminescent Probes. *J. Am. Chem. Soc.* **2004**, *126*, 15394–15395. [[CrossRef](#)]
7. Andruh, M.; Costes, J.-P.; Diaz, C.; Gao, S. 3d-4f Combined Chemistry: Synthetic Strategies and Magnetic Properties. *Inorg. Chem.* **2009**, *48*, 3342–3359. [[CrossRef](#)]
8. Wang, P.; Chen, W.; Xia, J. Synthesis, Structures, and Properties of Lanthanide Complexes with Pyrimidine-2-carboxylic Acid. *Z. Anorg. Allg. Chem.* **2017**, *643*, 1752–1758. [[CrossRef](#)]
9. Li, B.; Wen, H.-M.; Cui, Y.; Qian, G.; Chen, B. Multifunctional lanthanide coordination polymers. *Prog. Polym. Sci.* **2015**, *48*, 40–84. [[CrossRef](#)]
10. Colacio, E.; Rodríguez-Diéguez, A. Possibilities with 2-pyrimidinecarbonitrile to design MOFs. *Polyhedron* **2014**, *80*, 173–179. [[CrossRef](#)]
11. Zhang, J.-Y.; Yue, Q.; Jia, Q.-X.; Cheng, A.-L.; Gao, E.-Q. Syntheses, structures and luminescence properties of cadmium (II) coordination polymers with *in situ* formed oxalate and bis(chelating) bridging ligands. *Cryst. Eng. Comm.* **2008**, *10*, 1443–1449. [[CrossRef](#)]

12. Zhang, X.-M.; Zheng, Y.-Z.; LI, C.-R.; Zhang, W.-X.; Chen, X.-M. Unprecedented (3,9)-Connected $(4^2.6)_3(4^6.6^{21}.8^9)$ Net Constructed by Trinuclear Mixed-Valence Cobalt Clusters. *Cryst. Growth Des.* **2007**, *7*, 980–983. [[CrossRef](#)]
13. Long, D.-L.; Blake, A.J.; Champness, N.R.; Wilson, C.; Schröder, M. Unprecedented Seven- and Eight-Connected Lanthanide Coordination Networks. *Angew. Chem. Int. Ed.* **2001**, *40*, 2443–2447. [[CrossRef](#)]
14. Sun, R.; Gao, S.-M.; Wang, S.-Q.; Song, W.-C.; Zhao, J.-P.; Liu, F.-C. Co-ligand tuned pyrimidine-2-carboxylate Mn (II) complexes from a 2D 6^3 layer to an interpenetrated srs-net. *Dalton Trans.* **2017**, *46*, 8593–8597. [[CrossRef](#)] [[PubMed](#)]
15. Shen, L.; Yang, L.; Fan, Y.; Wang, L.; Xu, J. Construction of a series of lanthanide metal–organic frameworks: Synthesis, structure, luminescence and white light emission. *Cryst. Eng. Comm.* **2015**, *17*, 9363–9369. [[CrossRef](#)]
16. Jia, L.; Sun, H.-L.; Wang, Z. Crystal structures and luminescent properties of new lanthanide(III) complexes derived from 2-phenyl-4-pyrimidinecarboxylate. *RSC Adv.* **2015**, *5*, 96855–96861. [[CrossRef](#)]
17. Wang, Z.-N.; Xu, X.-T.; Lv, X.; Bai, F.-Y.; Liu, S.-Q.; Xing, Y.-H. Synthesis, crystal structure, fluorescence and antimicrobial activity of a series of rare-earth complexes based on indolebutyric acid. *RSC Adv.* **2015**, *5*, 104263–104274. [[CrossRef](#)]
18. Rodríguez-Diéguez, A.; Cano, J.; Kivekäs, R.; Debdoubi, A. and Colacio, Self-Assembled Cationic Heterochiral Honeycomb-Layered Metal Complexes with the in Situ Generated Pyrimidine-2-carboxylato Bisdidentate Ligand. Hydrothermal Synthesis, Crystal Structures, Magnetic Properties, and Theoretical Study of $[M_2(\mu\text{-pymca})_3]\text{OH}\cdot\text{H}_2\text{O}$ ($M = \text{FeII}, \text{CoII}$). *Inorg. Chem.* **2007**, *46*, 2503–2510. [[CrossRef](#)]
19. Suárez-Varela, J.; Mota, A.J.; Aouryaghal, H.; Cano, J.; Rodríguez-Diéguez, A.; Luneau, D.; Colacio, E. Anion Influence on the Structure and Magnetic Properties of a Series of Multidimensional Pyrimidine-2-carboxylato-Bridged Copper(II) Complexes. *Inorg. Chem.* **2008**, *47*, 8143–8158. [[CrossRef](#)]
20. Colacio, E.; Aouryaghal, H.; Mota, A.J.; Cano, J.; Sillanpää, R.; Rodríguez-Diéguez, A. Anion encapsulation promoted by anion/p interactions in rationally designed hexanuclear antiferromagnetic wheels: Synthesis, structure and magnetic properties. *Cryst. Eng. Comm.* **2009**, *11*, 2054–2064. [[CrossRef](#)]
21. Oyarzabal, I.; Ruiz, J.; Ruiz, E.; Aravena, D.; Seco, J.M.; Colacio, E. Increasing the effective energy barrier promoted by the change of a counteranion in a Zn-Dy-Zn SMM: Slow relaxation *via* the second excited state. *Chem. Commun.* **2015**, *51*, 12353–12356. [[CrossRef](#)]
22. Bruker. *Bruker AXS Inc. V2019.1*; Bruker: Madison, WI, USA, 2019.
23. Sheldrick, G.M. SHELXT-Integrated space-group and crystal-structure determination. *Acta Crystallogr. Sect. A* **2015**, *71*, 3–8. [[CrossRef](#)] [[PubMed](#)]
24. Sheldrick, G.M. Crystal structure refinement with SHELXL. *Acta Crystallogr. Sect. C* **2015**, *71*, 3–8. [[CrossRef](#)] [[PubMed](#)]
25. Dolomanov, O.; Bourhis, L.J.; Gildea, R.; Howard, J.A.; Puschmann, H. OLEX2: A complete structure solution, refinement and analysis program. *J. Appl. Crystallogr.* **2009**, *42*, 339–341. [[CrossRef](#)]
26. Spek, A.L. Single-crystal structure validation with the program PLATON. *J. Appl. Crystallogr.* **2003**, *36*, 7–11. [[CrossRef](#)]
27. Ruiz, E.; Cano, J.; Álvarez, S.; Alemany, P. Broken symmetry approach to calculation of exchange coupling constants for homobinuclear and heterobinuclear transition metal complexes. *J. Comput. Chem.* **1999**, *20*, 1391–1400. [[CrossRef](#)]
28. Frisch, M.J.; Trucks, G.W.; Schlegel, H.B.; Scuseria, G.E.; Robb, M.A.; Cheeseman, J.R.; Scalmani, G.; Barone, V.; Petersson, G.A.; Nakatsuji, H.; et al. *Gaussian 16*; Revision A.01; Gaussian, Inc.: Wallingford, UK, 2016.
29. Dennington, R.; Keith, T.; Millam, J. *GaussView*; Version 5; Semicem Inc.: Shawnee Mission, KS, USA, 2009.
30. Chilton, N.F.; Collison, D.; McInnes, E.J.; Winpenny, R.E.; Soncini, A. An electrostatic model for the determination of magnetic anisotropy in dysprosium complexes. *Nat. Commun.* **2013**, *4*, 2551–2558. [[CrossRef](#)]
31. O’Boyle, N.M.; Tenderholt, A.L.; Langner, K.M. cclib: A library for package-independent computational chemistry algorithms. *J. Comput. Chem.* **2008**, *29*, 839–845. [[CrossRef](#)]
32. Ruiz, C.; García-Valdivia, A.A.; Fernández, B.; Cepeda, J.; Oyarzabal, I.; Abas, E.; Laguna, M.; García, J.A.; Fernández, I.; San Sebastian, E.; et al. Multifunctional coordination compounds based on lanthanide ions and 5-bromonicotinic acid: Magnetic, luminescence and anti-cancer properties. *CrystEngComm* **2019**, *21*, 3881–3890. [[CrossRef](#)]
33. Noodleman, W.-G.H. Structural model studies for the high-valent intermediate Q of methane monooxygenase from broken-symmetry density functional calculations. *Inorg. Chim. Acta* **2008**, *361*, 973–986. [[CrossRef](#)]

34. Guo, F.-S.; Day, B.M.; Chen, Y.-C.; Tong, M.-L.; Mansikkamäki, A.; Layfield, R.A. Magnetic hysteresis up to 80 kelvin in a dysprosium metallocene single-molecule magnet. *Science* **2018**, *362*, 1400–1403. [[CrossRef](#)] [[PubMed](#)]
35. Ruiz, J.; Mota, A.J.; Rodríguez-Diéguez, A.; Titos, S.; Herrera, J.M.; Ruiz, E.; Cremades, E.; Costes, J.P.; Colacio, E. Field and dilution effects on the slow relaxation of a luminescent DyO9 low-symmetry single-ion magnet. *Chem. Commun.* **2012**, *48*, 7916–7918. [[CrossRef](#)] [[PubMed](#)]
36. Rinehart, J.D.; Long, J.R. Exploiting single-ion anisotropy in the design of f-element single-molecule magnets. *Chem. Sci.* **2011**, *2*, 2078–2085. [[CrossRef](#)]
37. Liu, J.-L.; Chen, Y.-C.; Zheng, Y.-Z.; Lin, W.-Q.; Ungur, L.; Wernsdorfer, W.; Chibotaru, L.F.; Tong, M.-L. Switching the anisotropy barrier of a single-ion magnet by symmetry change from quasi-D5h to quasi-Oh. *Chem. Sci.* **2013**, *4*, 3310–3316. [[CrossRef](#)]
38. García-Valdivia, A.; Zabala-Lekuona, A.; Goñi-Cárdenas, A.; Fernández, B.; García, J.A.; Quílez del Moral, J.F.; Cepeda, J.; Rodríguez-Diéguez, A. Dilution Effect on the Slow Relaxation of a Luminescent Dysprosium Metal-Organic Framework based on 2, 5-dihydroxyterephthalic acid. *Inorg. Chim. Acta* **2020**, *509*, 119687. [[CrossRef](#)]
39. Bünzli, J.C.G. On the design of highly luminescent lanthanide complexes. *Coord. Chem. Rev.* **2015**, *293*, 19–47. [[CrossRef](#)]
40. Heine, J.; Müller-Buschbaum, K. Engineering metal-based luminescence in coordination polymers and metal–organic frameworks. *Chem. Soc. Rev.* **2013**, *42*, 9232–9242. [[CrossRef](#)]



© 2020 by the authors. Licensee MDPI, Basel, Switzerland. This article is an open access article distributed under the terms and conditions of the Creative Commons Attribution (CC BY) license (<http://creativecommons.org/licenses/by/4.0/>).